Alkassar S, Woo WL, Dlay SS, Chambers J. **Robust Sclera Recognition System with Novel Sclera Segmentation and Validation Techniques**. *IEEE Transactions on Systems, Man and Cybernetics: Systems* 2016

Copyright:

Date deposited:

25/05/2016

Robust Sclera Recognition System with Novel Sclera Segmentation and Validation Techniques

S. Alkassar, *Student Member, IEEE,* W. L. Woo, *Senior Member, IEEE,* S. S. Dlay,
and J. A. Chambers, *Fellow, IEEE,*

Abstract—**Sclera blood veins have been investigated recently as a biometric trait which can be used in a recognition system. The sclera is the white and opaque outer protective part of the eye. This part of the eye has visible blood veins which are randomly distributed. This feature makes these blood veins a promising factor for eye recognition. The sclera has an advantage in that it can be captured using a visible-wavelength camera. Therefore, applications which may involve the sclera are wide ranging. The contribution of this paper is the design of a robust sclera recognition system with high accuracy. The system comprises of new sclera segmentation and occluded eye detection methods. We also propose an efficient method for vessel enhancement, extraction and binarization. In the feature extraction and matching process stages, we additionally develop an efficient method that is orientation, scale, illumination and deformation invariant. The obtained results using UBIRIS.v1 and UTIRIS databases show an advantage in terms of segmentation accuracy and computational complexity compared with state-of-art methods due to Thomas, Oh, Zhou and Das.**

Index Terms—**Biometrics, wavelet transforms, feature extraction, pattern recognition, sclera recognition**

I. INTRODUCTION

RECENT research on biometrics have shown an increased interest in new human traits rather than the typical biometrics [1]. Human recognition systems using blood vessel patterns for instance have been investigated using the retina [2], palms [3], fingers [4], conjunctival vasculature [5] and sclera [6]. The sclera can be defined as the white and opaque outer protective part of the eye. It consists of four tissue layers: the episclera, stroma, lamina fusca and endothelium [7] which surround the iris. The iris is the colored tissue around the pupil. This is shown in Fig. 1. The sclera has visible blood veins which are randomly distributed in different orientations and layers making them a promising factor for the improvement of an eye recognition system [8].

Typical sclera recognition systems involve sclera segmentation, blood vessel enhancement, feature extraction and a matching process which is shown in Fig. 2. In addition, a summary of recent published work on single sclera modality is given in Table I. Sclera segmentation has evolved from the manual segmentation applied by Derakhshani et al. [5], [9] which is an unreliable approach for real-time applications because of the human supervision required with the

S. Alkassar, W. L. Woo, S. S. Dlay and J. A. Chambers are with the School of Electrical and Electronic Engineering, Newcastle University, Newcastle Upon Tyne, NE1 7RU, UK (e-mails: {s.h.m.alkassar, Lok.Woo, Satnam.Dlay, Jonathon.Chambers}@newcastle.ac.uk). S. Alkassar is also a staff member with Electronics Engineering collage, University of Mosul, Iraq.

segmentation process and the expensive processing time. In the semi-automated method suggested by Crihalmeanu et al. [10] based on K-means clustering, the eyelids included in the resulting sclera image were manually corrected. After that, two automated strategies were suggested based on sclera pixel thresholding and a sclera shape contour to extract sclera regions. For the sclera pixel thresholding technique, Thomas et al. [11] and Zhou et al. [6], [12], [13] converted the color images into the HSV color space and the sclera region was extracted as it has low hue, low saturation and high intensity in the HSV space. Then, another mask was created from a skin detection method and the convex hull of each mask was calculated and fused for the final sclera mask. Oh and Toh [14] used the HSV color space with histogram equalization and lowpass filtering in order to extract the sclera. For grayscale images, Otsu's thresholding method was applied to detect sclera regions as the intensity of the sclera area is different from the background. In contrast, the sclera shape contour technique was utilized in [15]–[17] which depends on the convergence of the contours through the sclera region. A time-adaptive active contour was used to extract the sclera regions.

For the enhancement of blood vessels, Derakhshani et al. [5], [9] utilized Contrast-Limited Adaptive Histogram Equalization (CLAHE) with a region growing method to extract the binary network of the sclera blood vessels. A bank of Gabor filters was used in [6], [12], [13] whereas adaptive histogram equalization with the discrete Haar wavelet was used in [17] to enhance the vessel patterns. While for the feature extraction process, Zhou et al. [6], [12], [13] proposed a line segment descriptor based on the iris centroid. Oh and Toh [14] used an angular grid with Local Binary Patterns (LBP) whereas Derakhshani et al. [5], [9] suggested minutiae detection and a matching method for sclera recognition.

Several issues and challenges remain for sclera recognition which may affect the system performance. These are: 1) sclera segmentation with pixel thresholding could be affected by the
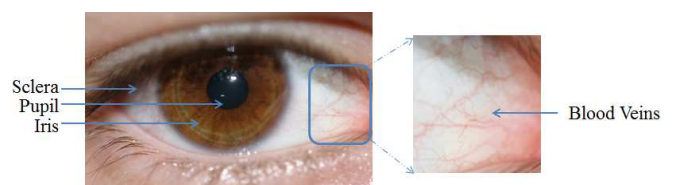

Fig. 1. Eye structure consisting of pupil, iris and sclera region.

TABLE I
RECENT WORKS RELATED TO SCLERA-BASED RECOGNITION USING A SINGLE SCLERA MODALITY

Authors	Year	Sclera segmentation	Vessels enhancement	Feature Extraction	Database(subj./img.)	Learning-based	The best performance
Derakhshani et al. [5]	2006	Manual	CLAHE[a], region growing method	Hu's invariant moments, minutiae[b]	In-house DB (6/12)	No	100% identification rate
Derakhshani et al. [9]	2007	Manual	CLAHE	CDF 9/7[c]	In-house DB(50/300)	Yes 3 TIPU[d]	4.3% EER
Crihalmeanu et al. [10]	2009	Semi-automated (pixel thresholding)	CLAHE, selective enahncement filter	Affine transform	In-house DB(50/100)	No	25% EER
Thomas et al. [11]	2010	Automated (pixel thresholding)	Gabor filters bank	Line segments description	UBIRIS.v1 (241/1205)	Yes 2 TIPU	3.38% EER
Oh and Toh [14]	2012	Automated (pixel thresholding)	-	Angular grid, LBP [e]	UBIRIS.v1 (241/1205)	No	0.47% EER
Zhou et al. [6]	2012	Automated (pixel thresholding)	Gabor filters bank	Line segments description	UBIRIS.v1 (241/1805)	Yes 2 TIPU	4.09% EER
Lin et al. [18]	2014	Automated (pixel thresholding)	Gabor filters bank	Line segments description	UBIRIS.v1 (241/1168)	Yes 2 TIPU	3.05% EER
Das et al. [17]	2013	Automated (shape contour)	AHE [f], Haar wavelet filters bank	D-SIFT [g]	UBIRIS.v1 (241/1205)	Yes 3 TIPU	0.66% EER
Das et al. [19]	2014	Automated (shape contour)	AHE, Discrete Meyer wavelet filters bank	LDP [h]	UBIRIS.v1 (241/1350)	Yes 5 TIPU	3.95% EER

[a] CLAHE: Contrast-Limited Histogram Equalization.
[b] Minutiae detection and matching.
[c] CDF 9/7: Cohen-Daubeches-Feauveau 9/7 wavelet.
[d] TIPU: Training images per user.
[e] LBP: Local Binary Pattern.
[f] AHE: Adaptive Histogram Equalization.
[g] D-SIFT: Dense Scale Invariant Feature Transform.
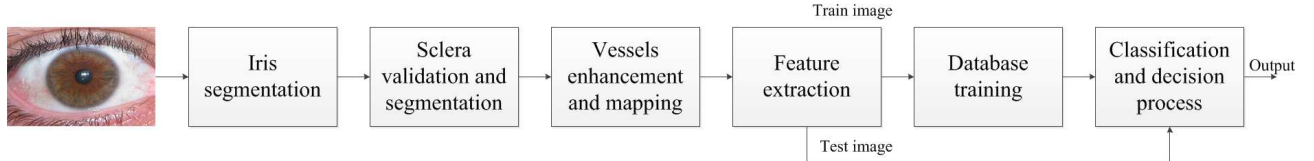[h] LDP: Local Directional Pattern.

Fig. 2.   Typical sclera recognition system design.

noise and distortion present in sclera images; 2) the effects of the sclera boundary on the convergence of the sclera shape contour; 3) occluded or partial occluded and noisy images are discarded manually; 4) the enhancement of blood vessels and the feature extraction algorithm should be invariant to nonlinear blood vessel movement [6]; 5) robust user template registration and an efficient matching procedure are required. To mitigate these limitations, we propose the following novel contributions to achieve a practical sclera recognition system based only on visible-wavelength illumination:

- Occluded eye image detection;
- Adaptive sclera shape contour segmentation based on active contours without edges;
- Efficient image enhancement and vessel map extraction;
- Robust sclera feature extraction with template registration and matching.

The organization of the paper is as follows: in Section II, we propose a new unsupervised sclera segmentation and occluded eye detection method. Section III discusses the enhancement, extraction, and mapping of blood vessels. Section IV includes the feature extraction process and user template registration while Section V discusses the matching and decision steps. In Section VI, we introduce our evaluation results and finally we present the conclusions in Section VII.

II. PROPOSED SCLERA SEGMENTATION

Sclera segmentation is the initial and the most challenging step in a sclera recognition system. The accuracy of the sclera recognition system could be degraded if the segmentation process fails to extract the correct sclera regions from an eye image. Some incorrect sclera segmentation scenarios include segmenting the sclera with some parts of the iris, eyelids and eyelashes. Table I shows sclera segmentation techniques developed from both manual and automated segmentation processes. Two strategies, sclera pixel thresholding and sclera shape contour, have been adopted each having their advantages and disadvantages. We will focus on the sclera shape contour technique in this paper as the sclera pixel thresholding involves multiple steps to remove noise and segmenting sclera region, thus increasing the complexity and processing time. We propose an adaptive approach for unsupervised fully automated sclera segmentation by using active contours without edges [20] with a novel occluded eye detection method.

A. Iris Segmentation

Iris center estimation has an essential role in our proposed sclera segmentation method. Although the sclera recognition system does not depend directly on the iris for the system implementation. However, locating the position of the iris center within the eye image plays a crucial part in our proposed sclera segmentation. There is a significant amount of literature

on iris segmentation [21]–[25] for which the iris region is modeled as circular boundaries and it is not our focus area to improve these methods rather than to extract the iris center and radius. We use the integro-differential operator suggested by Daugman [21] which acts as a circular edge detector. The integro-differential operator is defined as

$$\arg \max_{(r,x_0,y_0)} \left| G_\sigma\left(r\right) * \frac{\partial}{\partial r} \oint_{r,x_0,y_0} \frac{I\left(x,y\right)}{2\pi r} ds \right|, \qquad (1)$$

where $I\left(x,y\right)$ is the grayscale level of the eye image, (r,x_0,y_0) are the iris radius and center coordinates, the symbol $*$ is the convolution operator and $G_\sigma\left(r\right)$ is a Gaussian smoothing function of scale σ. The colored image is first converted into grayscale format and down-sampled by factor of 0.25 to enhance the processing time. This is shown in Fig. 3.
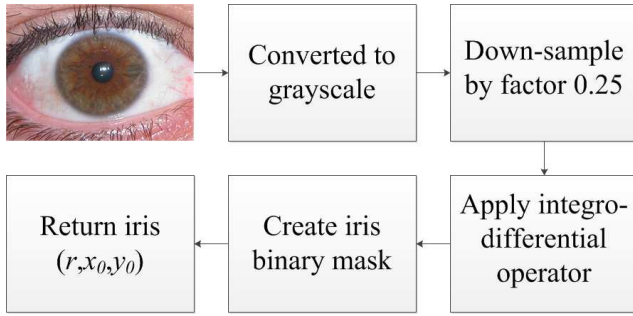

Fig. 3. Iris segmentation process.

B. Occluded Eye Detection For Sclera Validation

One major challenge in the sclera segmentation process is the sclera validation where the segmented sclera is automatically verified without any supervision from the human. There are some factors such as an occluded eye image and small sclera area which will affect the automation process and increase error rate. Many researchers have discarded these images manually or applied sclera validation after the sclera segmentation step. However, if the sclera image has an occluded eye, then validating the sclera after segmentation is inefficient. Therefore, we propose a sclera validation process by isolating the poor samples in the enrollment and verification stages. The proposed method is applied before sclera segmentation to detect partial or fully occluded eye image, to make a validation decision of a sufficient sclera region.

Based on the iris radius and center coordinates (r,x_0,y_0), two arc areas of intensities are specified according to the following

$$\mathbf{Arc} = RGB\left(x_0 + r\cos\theta, y_0 + r\sin\theta\right), \qquad (2)$$

where $\theta \in [-\pi/3 : \pi/3] \cup [-2\pi/3 : 2\pi/3]$ with uniform increment steps of 0.1 degree and is set in this range to check the status where eyelids are partially closed. Then, the RGB intensities of each pixel in these two arc areas have been classified by heuristic rules into a skin or not-skin labels using the Color Distance Map (CDM) proposed in [26]. First, we will explain this method by applying it on the right arc

$\mathbf{Arc}_r$ and the same operation will be applied on the left arc $\mathbf{Arc}_l$. First, two skin clusters for natural illumination and flash illuminator conditions are defined as

$$CDM_1 = \begin{cases} 1, & \begin{aligned} &R > 95, G > 40, B > 20, \\ &\max\left(R,G,B\right) - \min\left(R,G,B\right) > 15, \\ &|R - G| > 15, R > G, R > B \end{aligned} \\ 0, & \text{otherwise} \end{cases}, \qquad (3)$$

$$CDM_2 = \begin{cases} 1, & \begin{aligned} &R > 220, G > 210, B > 170, \\ &|R - G| \le 15, B < R, B > G. \end{aligned} \\ 0, & \text{otherwise} \end{cases} \qquad (4)$$

Then, the non-skin map is created based on these clusters as

$$\mathbf{s}_r(i) = \begin{cases} 1, & \text{if } CDM_1(i) \parallel CDM_2(i) = 0 \\ 0, & \text{otherwise} \end{cases}, \qquad (5)$$

where the symbol $\parallel$ refers to the logical OR operator, 1 refers to a non-skin pixel and 0 to a skin pixel. The same operation will be repeated on $\mathbf{Arc}_l$ to produce $\mathbf{s}_l$. Next, from the $\mathbf{s}_r$ and $\mathbf{s}_l$ vectors, four sub-arcs $\mathbf{up}_r$ with $\Theta \in [\pi/6 : \pi/3]$, $\mathbf{up}_l$ with $\Theta \in [5\pi/6 : 2\pi/3]$, $\mathbf{down}_r$ with $\Theta \in [-\pi/6 : -\pi/3]$ and $\mathbf{down}_l$ with $\Theta \in [-5\pi/6 : -2\pi/3]$ are used to define decision parameters for the non-skin pixels as

$$\mathbf{nsk}_{up}(i) = \mathbf{up}_r(i) \bigcap \mathbf{up}_l(i), \qquad (6)$$

$$\mathbf{nsk}_{down}(i) = \mathbf{down}_r(i) \bigcap \mathbf{down}_l(i), \qquad (7)$$

where $\bigcap$ is the logical AND operator and Θ is set within this range empirically to enhance the processing time. Then, the percentage of the non-skin pixels is calculated for both $\mathbf{nsk}_{up}$ and $\mathbf{nsk}_{down}$ as

$$per_{\mathbf{nsk}_{up}} = \frac{\text{No. of } 1s \ (\mathbf{nsk}_{up})}{\text{Total No. of elements } (\mathbf{nsk}_{up})}, \qquad (8)$$

$$per_{\mathbf{nsk}_{down}} = \frac{\text{No. of } 1s \ (\mathbf{nsk}_{down})}{\text{Total No. of elements } (\mathbf{nsk}_{down})}. \qquad (9)$$

According to $per_{\mathbf{nsk}_{up}}$ and $per_{\mathbf{nsk}_{down}}$, the final decision to accept or reject the eye image is defined as

$$\text{Eye image} = \begin{cases} \text{Accept}, & \text{if } per_{\mathbf{nsk}_{up}} \ge 0.6 \ \bigcap \ per_{\mathbf{nsk}_{down}} \ge 0.3 \\ \text{Reject}, & \text{otherwise} \end{cases}, \qquad (10)$$

where 0.6 and 0.3 are set empirically for optimum performance. After that, if the eye image is validated for a sufficient sclera area, then the iris binary mask is applied to segment the iris and the image is ready for the sclera segmentation. Otherwise, no further processing time is required and the image is rejected. The proposed validation process for an ideal eye and partial occluded eye images is shown in Fig. 4.
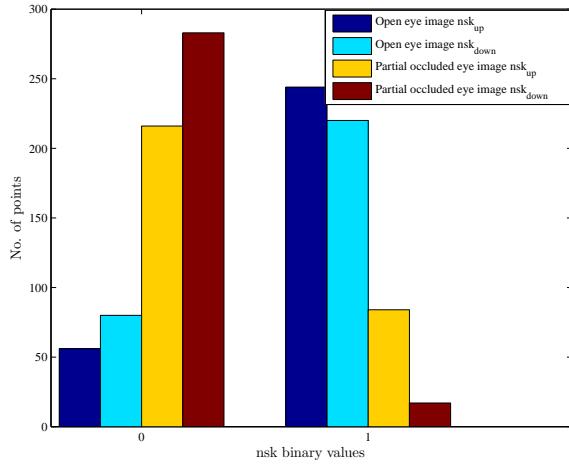
C. Sclera Segmentation

Having presented the sclera validation methodology, we next describe the proposed full procedure for sclera segmentation.
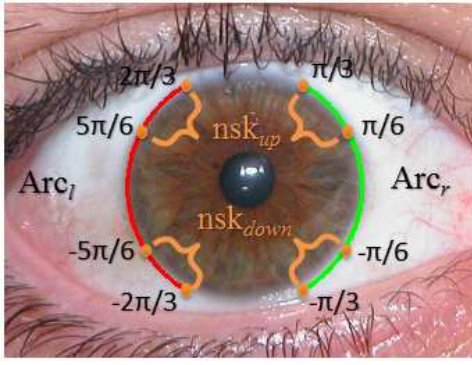
(a)
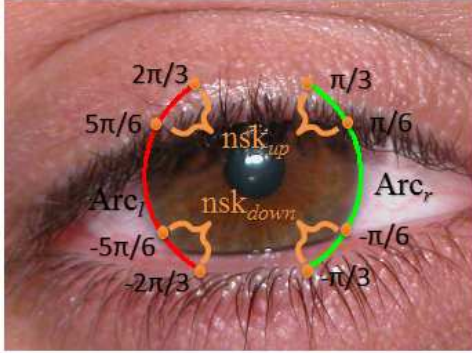
(b)

(c)

Fig. 4. Proposed occluded and partially occluded eye image detection, (a) and (b) are an ideal eye image and partial occluded eye image respectively with the angles depicted where $\mathbf{nsk}_{up}$ and $\mathbf{nsk}_{down}$ are calculated, (c) the histograms of skin and non-skin pixels in the $\mathbf{nsk}_{up}$ and $\mathbf{nsk}_{down}$ vectors.

1) Seed-base Initialization of Contours: For a frontal-looking iris, two initial seeds for the left and right contours are initialized depending on the iris radius and center coordinates (r, x_0, y_0). The center positions of these seeds are calculated as
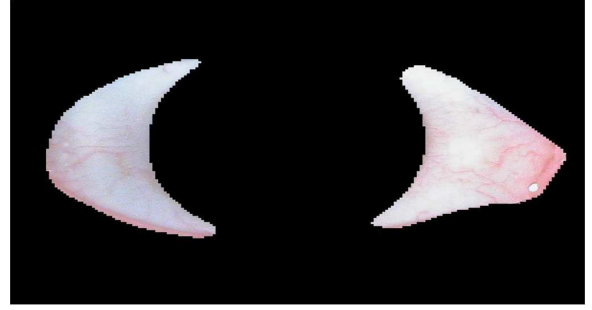
$$C_{rs}(x, y) = (x_0 + (1.35 \times r), y_0), \qquad (11)$$

and

$$C_{ls}(x, y) = (x_0 - (1.35 \times r), y_0), \qquad (12)$$
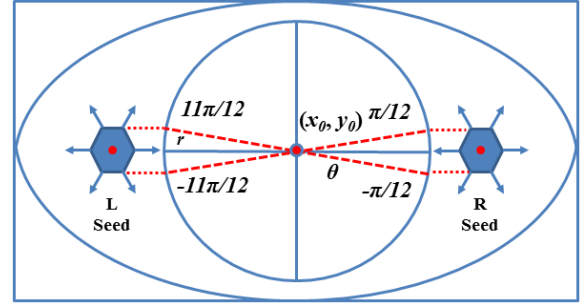
(a)

(b)

Fig. 5. Segmentation process for the sclera, (a) initial seeds for the right and left contours for iris-centered eye, (b) sclera segmented template.

where $1.35 \times r$ is set to ensure that the right and left seed centers are outside the iris. The height of the initial contours is set with altitude from the point on the iris circumference with $\theta = \pi/12$ to the point with $\theta = -\pi/12$ and the width $(r/2)$ to make the contours converge inside the sclera regions. The initial seed positions are depicted in Fig. 5a.

2) Active Contours Without Edges: The basic idea in snakes or active contour models is to develop a curve subject to image forces in order to detect salient objects [27]–[30]. For instance, a curve is initialized around an object to be detected and the curve will move towards that object until its boundary is detected. However, a major problem with these active contour models is that they have to rely on an edge function which depends on the image gradient. These models can detect only objects with edges defined by the gradients that stop the curve evolution. In practice, the discrete gradients are bounded. Therefore, the stopping function is never zero on the edges and the curve may pass through the boundary. Another problem is that if the image is contaminated with noise, it will require a strong isotropic smoothing Gaussian function to remove the noise at the cost of smoothing the edges as well.

In contrast, the active contours without edges model [20] has no stopping edge function i.e., the gradient of the image is not adopted for the stopping process, instead the Mumford-Shah segmentation techniques are adopted [31]. The advantage of this model is the ability of detecting contours independent of gradients. For instance, objects with very smooth boundaries or with discontinuous boundaries.

Summarizing the development in [20], let an eye image in the grayscale I_0 be an open subset of $\mathbb{R}^2$ with its boundary equals ∂I_0, and the evolving curve C in I_0 representing the boundary of sclera ω of I_0 i.e., $\omega \subset I_0$ and $C = \partial \omega$. Then, the

terms $inside(C)$ and $outside(C)$ will equal the area regions of ω and $I_0 \backslash \bar{\omega}$ respectively, where the symbol $(\backslash)$ denotes removal of the ensuing term and $\bar{\omega}$ is the closed region of ω. Assuming that I_0 has two regions of approximately piecewise-constant intensities I_0^i and I_0^o, then the sclera to be detected is the region with value I_0^i. The fitting term of the active contour model is represented by the energy function $F(c_1, c_2, C)$ which is minimized if the curve C is on the boundary of ω and defined as

$$F(c_1, c_2, C) = F_1(C) + F_2(C) + \mu.Length(C) \\ + \nu.Area(inside(C)), \quad (13)$$

where $F_1(C)$ and $F_2(C)$ equal

$$F_1(C) = \lambda_1 \int_{inside(C)} |I_0(x,y) - c_1|^2 \, dxdy, \quad (14)$$

$$F_2(C) = \lambda_2 \int_{outside(C)} |I_0(x,y) - c_2|^2 \, dxdy, \quad (15)$$

where $\mu \geq 0$, $\nu \geq 0$, $\lambda_1, \lambda_2 > 0$ are fixed parameters, and c_1, c_2, are the averages of I_0 inside and outside C respectively. Further details of the minimizing procedure is in [20]. The parameters $\lambda_1, \lambda_2 = 1$ and $\nu = 0$ are fixed for best performance whereas the time step Δt is set to 0.1. μ is the controlling parameter of the evolving curve C. The smaller the value of μ, the more ability to detect as many objects as possible with different sizes. As μ increases, the curve C will detect only large objects. In our case, we set μ empirically high to 0.2 in order to not detect the blood veins inside the sclera rather the sclera boundary.

Then, the iris-segmented image is converted to the blue channel and down-sampled by factor = 0.2 to enhance processing time and the final sclera binary map is created. The initial contours will converge towards the sclera boundaries in all direction and will stop for a number of iterations $i = 200$. The final sclera template is shown in Fig. 5b.

III. SCLERA BLOOD VESSEL ENHANCEMENT AND MAPPING

The main purpose of the vessel enhancement is to isolate the blood vessels in the sclera from their background. This process has two stages. In the first stage, the green layer of the RGB image is extracted as it leads to better contrast between the sclera blood vessel and the background [32]. Then, CLAHE was applied to the sclera regions as it will enhance the green layer of the colored image [5].

For the vessel extraction, which is the second stage, we propose the two-dimensional Isotropic Undecimated Wavelet Transform (IUWT) as it is robust and well adapted to astronomical data and biology images where objects are more or less isotropic [33]. To extract $\mathcal{W} = \{w_1, \cdots, w_J, c_J\}$, where w_j are the wavelet coefficients at scale j and c_J are the coefficients at the coarsest resolution, a subtraction between two adjacent sets of coefficient scales is applied as

$$w_{j+1}[k,l] = c_j[k,l] - c_{j+1}[k,l], \quad (16)$$

where

$$c_{j+1}[k,l] = \left(\bar{h}^{(j)} \bar{h}^{(j)} * c_j \right)[k,l], \quad (17)$$

and $\bar{h}^{(j)}[k] = \frac{[1,4,6,4,1]}{16}$ is the non-orthogonal Astro filter bank with $k = -2, \cdots, 2$. At each scale j, one wavelet set is obtained which has the same resolution as the sclera image. This feature solves the dimensionalty increment introduced using Gabor filters with different scales and orientations and produces efficient processing time. The reconstruction process is obtained by co-addition of j wavelet scales as:

$$c_0[k,l] = c_J[k,l] + \sum_{j=1}^{J} w_j[k,l]. \quad (18)$$

The segmentation process for the vessels can be initiated simply by adding the best wavelet levels with a thresholding process that represents the best vessels contrast. The threshold to detect the vessels is empirically set to identify the lowest 30% of the coefficients. It is likely to misclassify non-vessel pixels as a vessel pixel. However, a cleaning process can be achieved simply by calculating the area of misclassified pixels and set a threshold to remove these undesired pixels. This is shown in Fig. 6a

The thickness variation in the sclera vessels due to the physiological status of a person [6] affects the recognition process. Therefore, these vessels must be transformed to a single pixel skeleton map. For the thinning process, a morphological thinning algorithm was applied and binary morphological operations are applied to remove the exterior pixels from the detected vascular vessels map and to create a one-pixel skeleton running along the center of the vessels. The binary skeleton map of the sclera vessels is shown in Fig. 6b.

IV. SCLERA FEATURE EXTRACTION AND TEMPLATE REGISTRATION

A. Sclera Feature Extraction

The feature extraction process in the sclera recognition system involves producing a reliable mathematical model in order to identify individuals. We propose a new method for the sclera pattern feature extraction based on Harris corner and edge detection [34]. This algorithm detects the Interest-Points
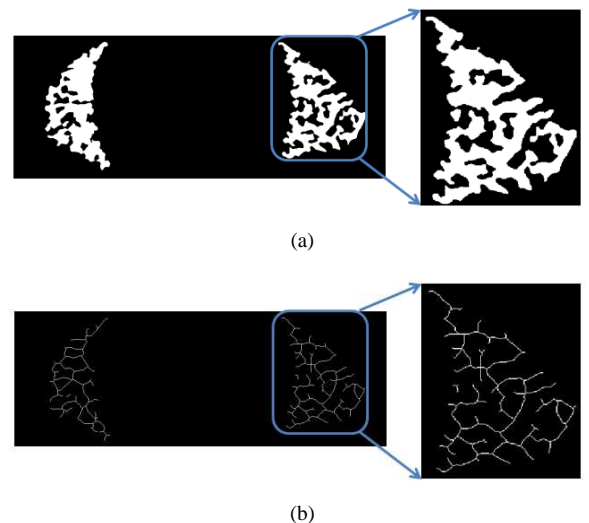

(a)

(b)

Fig. 6. The sclera blood vessels enhancement and mapping, (a) apply IUWT for the vessel extraction, (b) the morphological thinning process.
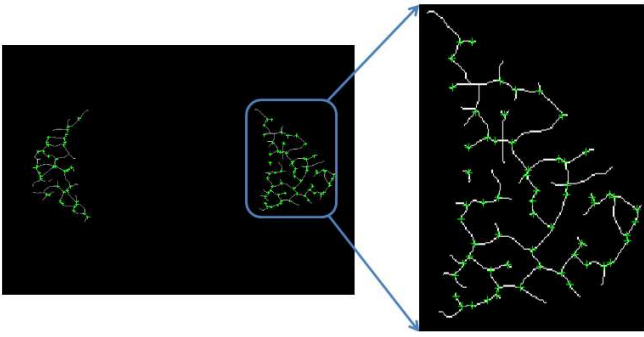
Fig. 7. Applying Harris detector to extract IP features.

(IPs) represented by the corner response R. Some of these IPs include Y, T, L and X vessel corner formations which supply a significant 2D texture for pattern recognition.

The corner response R is defined as

$$R = \det(A) - k \ \mathrm{tr}^2(A), \qquad (19)$$

where det is the determinant of matrix A, k is a constant set to 0.04, tr is the matrix trace and A is the image structure matrix computed from the image derivatives as

$$A = \begin{bmatrix} I_x^2 & I_x I_y \\ I_x I_y & I_y^2 \end{bmatrix}, \qquad (20)$$

where I_x and I_y are the partial derivatives in x and y respectively. The corner response value is positive when a corner region is detected, small if a flat region is detected and negative if an edge region is detected within the smooth circular Gaussian window. The steps for the IP extraction process is as follows

1) compute the 1st derivatives in x and y;
2) apply the Gaussian smoothing filter to remove the noisy response due to a binary window function;
3) find the points with a large corner response function R when $(R > th_C)$;
4) take the points of local maxima of R.

where th_C is set to 0.01 for best performance. The extracted IPs in the sclera vessel map are shown in Fig. 7.

After the IP locations have been extracted, the characteristic information such as the magnitude, phase and orientation within a specific window surrounding each feature point are calculated. We exploit the two-dimensional monogenic signal method [35] to extract the local information of these IPs. An analytic signal is constructed by using the Riesz transform. The analytic signal is isotropic and therefore provides a split of identity where the information is orthogonally decomposed into geometric and energetic information for the blood veins IPs in term of local amplitude, local phase and local orientation. If the coordinates of the vertical and horizontal filters are $\mathbf{u} = (u_1, u_2)$, then the Riesz kernels in the frequency domain are multiplied with Log-Gabor scale mask to calculate the spatial representation of the vertical and horizontal filters respectively as

$$h_1(\mathbf{u}) = i \frac{u_1}{|\mathbf{u}|} G(|\mathbf{u}|), h_2(\mathbf{u}) = i \frac{u_2}{|\mathbf{u}|} G(|\mathbf{u}|), \qquad (21)$$

where $|\mathbf{u}| = \sqrt{u_1^2 + u_2^2}$ represents the radius of frequency values from the center and $G(|\mathbf{u}|)$ is the monogenic scale space defined by using the Log-Gabor filter for a wavelength $1/f_0$ as

$$G(|\mathbf{u}|) = \exp\left(-\frac{(\log(|\mathbf{u}|/f_0))^2}{2(\log(k/f_0))^2}\right), \qquad (22)$$

where $1/f_0 = 0.1$ and $k = 0.2$ is the ratio of the standard deviation of the Gaussian describing the log-Gabor filter's transfer function in the frequency domain to the filter center frequency. If $f(I)$ represents the input image in the frequency domain, then the monogenic signal of input image $f_M(I)$ can be defined as

$$f_M(I) = f(I) + h(\mathbf{u}) * f(I), \qquad (23)$$

where $*$ is the convolution operator. For the monogenic signal representation in the image domain, 3-tuple variable $\{p(I), q_1(I), q_2(I)\}$ is defined as

$$\begin{aligned} p(x) &= (f * G_a)(I) \\ q_1(x) &= (f * h_1)(I), \\ q_2(x) &= (f * h_2)(I) \end{aligned} \qquad (24)$$

where G_a is the Log-Gabor filter of the image domain. The amplitude information is ignored as the vessel image is a binary form whereas the monogenic phase $\varphi(I)$, which will be in range $-\pi/2 \leq \varphi \leq \pi/2$, is calculated as

$$\varphi(I) = \tan^{-1} \frac{p(I)}{\sqrt{q_1(I)^2 + q_2(I)^2}}. \qquad (25)$$

Finally for each IP location, a window patch with size of (19×19) pixels is stored along with the analytic signal information and the sclera template will consist of the following components

$$\mathbf{St} = \{\text{IP.locations}, \text{IP.phases}\}. \qquad (26)$$

B. Sclera Feature Template Registration

The investigation of non linear blood vein movement in the sclera carried out by Zhou et al. [6] has shown that these vessels move slightly as the eye moves. To overcome this limitation and produce an invariant-blood movement user template, we propose a new method for user template registration. This method is initiated with the alignment of user sclera templates to a reference point. For the three training templates $\mathbf{St}_1$, $\mathbf{St}_2$ and $\mathbf{St}_3$, the reference points are $r_1(x, y)$, $r_2(x, y)$ and $r_3(x, y)$ which represent the radius of the iris. Then, these templates are aligned as follows

1) let $r_1(x, y)$ be the point where $\mathbf{St}_2$ and $\mathbf{St}_3$ are to be aligned;
2) for $\mathbf{St}_2$, subtract $(r_1(x, y), r_2(x, y))$ to extract the shift values (hr, vr) in the horizontal and vertical dimensions;
3) apply a circular shift where $\mathbf{St}_2$ is shifted in both directions as $\mathbf{St}_2(x + hr, y + vr)$;
4) repeat for $\mathbf{St}_3$.

If (hr, vr) are positive, $\mathbf{St}_2$ is shifted to the right and to the bottom, if (hr, vr) are negative, $\mathbf{St}_2$ is shifted to the left and to the top, if (hr) is positive and (vr) is negative, $\mathbf{St}_2$ is shifted
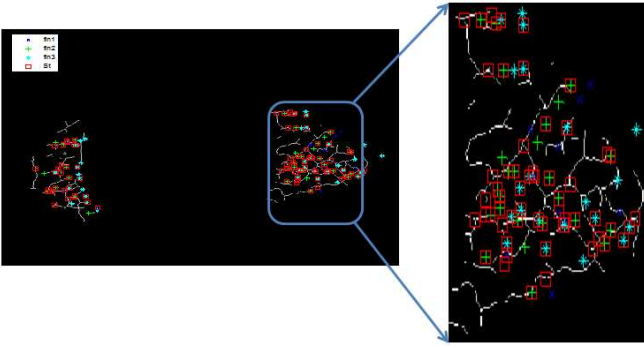
Fig. 8. The most homogeneous feature sets $\mathbf{St}^f$ represented in the red square extracted from $\mathbf{f_{in1}}$, $\mathbf{f_{in2}}$ and $\mathbf{f_{in3}}$.

to the right and to the top, and if (hr) is negative and (vr) is positive, $\mathbf{St}_2$ is shifted to the left and to the bottom.

Next, we propose a new method for feature matching based on a local descriptor to generate putative matching pairs $\mathbf{p_m}$ between these sclera feature sets, and Random Sampling Consensus (RANSAC) [36] to select the homogeneous feature sets $\mathbf{f_{in}}$. RANSAC uses the minimum number of feature points to estimate the initial feature sets and proceed to maximize the number of pairs within the set with consistent data points and thus decreasing the processing time. The proposed local descriptor includes generating a correlation matrix between two sclera templates $(\mathbf{St}_1, \mathbf{St}_2)$. The correlation matrix holds the correlation strength of every feature set in $\mathbf{St}_1$ relative to $\mathbf{St}_2$. Then, search for $\mathbf{p_{m1}}$ pairs that correlate maximally in both directions; $\mathbf{p_{m1}}$ can be calculated as

1) set a radius for the correlation window $rc = \frac{w-1}{2}$;
2) calculate the distances of $\mathbf{St}_1.\text{IP.location}(i)$ with all $\mathbf{St}_2.\text{IP.location}$;
3) specify the pairs points that have a distance $< d_{max}$;
4) normalize the phase information of the selected pairs points window to a unit vector form and measure the correlation using a dot product;
5) find $\mathbf{p_{m1}} = \arg\{\max |corr\,(\mathbf{St}_1, \mathbf{St}_2)$.

where d_{max} is set empirically to 50 for best performance.

Once the $\mathbf{p_{m1}}$ pairs for these templates were specified, then the process of finding $\mathbf{f_{in1}}$ for $\mathbf{p_{m1}}$ can be defined as follows

1) select randomly the minimum number of feature points $m = \arg\{\min(\mathbf{p_{m1}})\}$;
2) normalize each set of points so that the origin is at centroid and mean distance from origin is $\sqrt{2}$;
3) calculate Sampson error distances [37] between these sets and determine how many feature points from the templates fit with predefined Sampson error tolerance $< \epsilon$, where ϵ empirically set to 0.002.;
4) if the ratio of the number of $\mathbf{f_{in1}}$ over the total number of $\mathbf{p_{m1}}$ exceeds a predefined threshold b, re-estimate the model parameters using all the identified $\mathbf{f_{in1}}$ and terminate.
5) otherwise, repeat steps 1 through 4 for a maximum of N iterations.

The decision to stop selecting new feature subsets is based on the number of iterations N required to ensure that the

probability $z = 0.99$ that choosing random samples has at least one set does not include $\mathbf{f_{out}}$ points. N can be set as

$$N = \frac{\log(1-z)}{\log(1-b)}, \tag{27}$$

where $b = 1 - \left(\frac{\text{No. of } \mathbf{f_{in}}}{\text{No. of } \mathbf{p_m}}\right)^s$ represents the probability that any selected feature points is $\mathbf{f_{in1}}$ feature points and $s = 8$ is the number of points needed to fit a fundamental matrix [36]. This method uses a minimum number of feature points to estimate the homogeneous pairs set and maximizes this set with consistent feature points. After $\mathbf{f_{in1}}$, $\mathbf{f_{in2}}$ and $\mathbf{f_{in3}}$ have been extracted and grouped in one set, the final sclera user template $\mathbf{St}^f$ is created by removing the duplicated points. This is shown in Fig. 8. The angles ϕ between $\mathbf{St}^f$ points and iris center have been calculated for each point which will be used in the matching process to mitigate some outlier points been paired incorrectly.

V. SCLERA MATCHING AND DECISION PROCESS

The matching and decision process between two sclera templates is the final stage where the $\mathbf{St}^f$ of an enrolled user is compared in terms of local orientation and local phase with $\mathbf{St}^t$ of any test template. First, the putative feature sets $\mathbf{p_m}$ are extracted from $\mathbf{St}^f$ and $\mathbf{St}^t$. Then these pair sets are compared in term of the location and the angle to iris center. For the decision process, we propose a two stage decision method by using the Euclidean distance and the angle difference to classify the matching results. For each pair, two parameters are defined as

$$D_p = \begin{cases} 1, & \text{if } dist\left(\mathbf{St}^f, \mathbf{St}^t\right) \leq th_p \\ 0, & \text{otherwise} \end{cases}, \tag{28}$$

$$D_\phi = \begin{cases} 1, & \text{if } |\phi_f - \phi_t| \geq th_\phi \\ 0, & \text{otherwise} \end{cases}, \tag{29}$$

where $th_p = 20$ and $th_\phi = 5$ degrees are set empirically for best performance. The decision to accept or reject each pair is shown in Algorithm 1.

Finally, the decision process is calculated as

$$D_f = \begin{cases} Accept, & \text{if } \frac{\text{no. of accepted pairs}}{\text{no. of } \mathbf{p_m}} \geq th_f \\ Reject, & \text{otherwise} \end{cases}, \tag{30}$$

Algorithm 1: Decision process between two sclera template pairs

---

if $(D_\phi == 1)$ **then**
  if $(D_p == 1)$ **then**
    | Pair accepted;
  else
    | Pair rejected;
  end
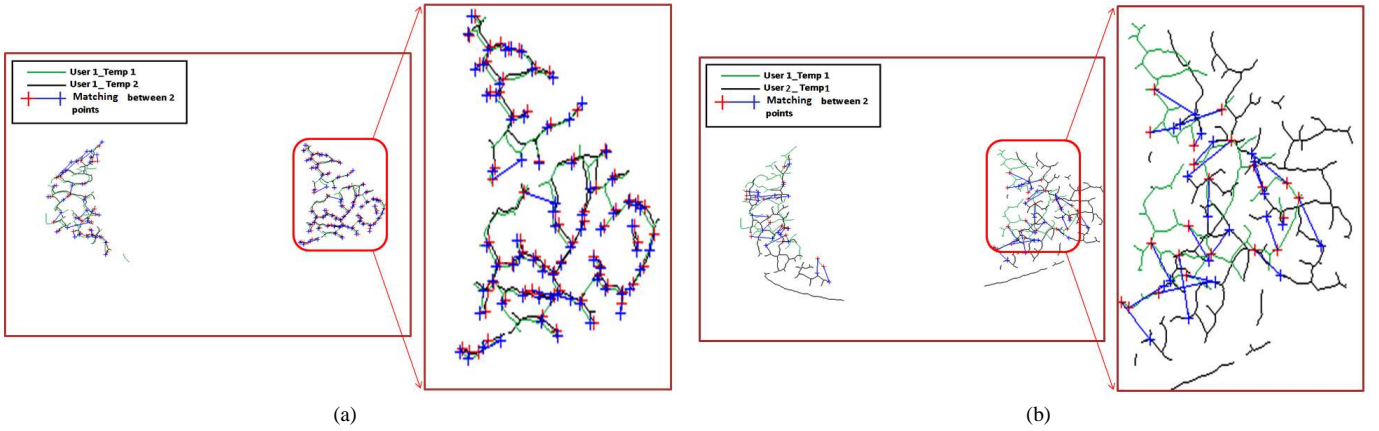**else**
  | Pair rejected;
end

Fig. 9. Examples of the matching process output between two sclera templates, (a) matching process between two sclera templates belonging to the same individual, (b) matching process between two sclera templates belonging to a different individuals.

where th_f is set empirically to 0.6.

Some examples of the matching results between two users are shown in Fig. 9. $\mathbf{p_m}$ points are represented by a red cross and $\mathbf{f_{in}}$ are in a blue cross. The matching between two sclera templates belonging to the same individual is shown in Fig. 9a whereas Fig. 9b shows the matching between two sclera templates belonging to different individuals. D_f is dramatically higher ($D_f = 89.51\%$) when matching two sclera templates for the same user than matching different user templates ($D_f = 49\%$).

VI. EXPERIMENTAL RESULTS

A. Experimental Methodology

The evaluation of a biometric system basically includes calculating the False Acceptance Rate (FAR), the False Rejection Rate (FRR) and the Equal Error Rate (EER) [38]. FAR and FRR are defined as

$$FAR = \frac{FP}{FP + TN} \times 100\%, \qquad (31)$$

$$FRR = \frac{FN}{FN + TP} \times 100\%, \qquad (32)$$

where FP is the false positive match, TP is the true positive match, FN is the false negative match and TN is the true negative match. EER denotes the error rate at threshold t where $FAR(t) = FRR(t)$. In addition, we used the Receiver Operating Characteristic (ROC) curve to evaluate the performance of our system where ROC is a plot of the FAR versus the Genuine Acceptance Rate (GAR). GAR is calculated as

$$GAR = 1 - FRR. \qquad (33)$$

B. Experimental Results Using the UBIRIS database

We utilized the UBIRIS.v1 database [39] to evaluate the performance of our proposed method. This database is composed of 1877 eye RGB images collected from 241 individuals in two sessions. In the first session which consists of 1214 images from 241 users, noise factors such as reflections, luminosity
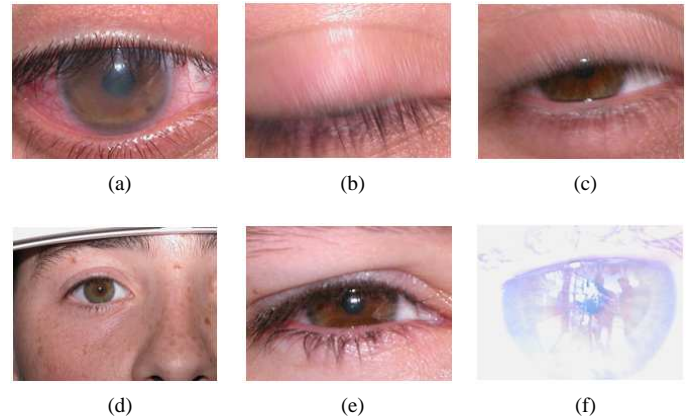

Fig. 10. UBIRIS.v1 database poor quality images. (a) an iterated sclera, (b) occluded eye, (c) partially occluded eye, (d) uncropped eye image, (e) insufficient sclera region and (f) high light exposure image.

and contrast were minimized as the images were captured inside a dark room. While in the second session which is composed of 663 images and involved only 135 from the 241 users, capturing location was changed in order to introduce a natural luminosity factor which introduced more reflections contrast, luminosity and focus problems. The UBIRIS.v1 database includes the images captured by a vision system with or without minimizing the collaboration of the subjects. Some images have a poor quality condition such as irritated sclera, closed eye, severe blurring, uncentered uncropped eye-area and poor lighting. Examples are shown in Fig.10. The evaluation process has been achieved in single-session and multi-session contexts. For the single-session context, we used 3 images for training and 2 for testing per user whereas the multi-session scenario uses session 1 images for training and session 2 images for testing and vise versa.

1) Sclera Validation Method Evaluation: The performance of the proposed sclera validation is measured by computing the Correct Sclera Validation (CSV) rate where the correct validation images are subjectively evaluated against the eye image decision in (10) and CSV is calculated as

$$CSV = \frac{\text{Number of } CAS + \text{Number of } CRS}{\text{Total number of images}} \times 100\%, \qquad (34)$$

TABLE II
THE CORRECT SCLERA VALIDATION RATE ON UBIRIS.V1

CSV	Session 1	Session 2
	95.38%	89.45%

where CAS is the Correctly Accepted Sclera image and CRS is the Correctly Rejected Sclera image. As shown in Table II, our proposed method has removed the partial or full occluded images and thus avoids expensive processing times and any human intervention. However, some limitations in our method can be concluded as follows 1) the detection process depends on the skin detection algorithm which is specifically designed for RGB images and thus, the inability to use it on grayscale images; 2) the process of finding $\mathbf{Arc}_r$ and $\mathbf{Arc}_l$ depends dramatically on the iris segmentation algorithm for the iris center. Therefore, the failure in extracting the iris center will cause errors in the validation process.

2) Active Contour Methods For Sclera Segmentation Comparison: We compared our proposed sclera segmentation method using active contours without edges with state-of-the-art active contour models such as the geodesic [30], balloons [40] and the gradient vector flow [41] active contours in term of accuracy and complexity as shown in Table III. We used Matlab (version R2013a) on a PC with Intel core i5 3.0 GHz processor and 8.0 GB RAM for implementing these algorithms. Our proposed algorithm is tended to focus on computer-based application and thus the hardware complexity is not discussed. For a fair comparison, the number of iterations in all models is set to 200 and the sclera images are down-sampled with factor = 0.2. For the subjective evaluation results as shown in Fig. 12, our proposed method overcomes the active contour model problem by not relying on the edge function which depends on the image gradient to stop the curve evolution. These drawbacks appear severely in noisy images and in the case of irregular sclera shape. In term of accuracy, our adapted method achieved 98.65% for Session 1 and 95.3% for Session 2 which is significantly higher than other active contour methods. In addition, our proposed method presented significantly lower processing time among these methods

TABLE III
COMPARISON OF SCLERA SEGMENTATION USING DIFFERENT ACTIVE
CONTOUR MODELS IN TERM OF ACCURACY AND COMPLEXITY ON
UBIRIS.V1

Session	Active Contours Method	Correctly Segmented Sclera Images	Processing Time
Session 1	Geodesic Active Contour [30]	68.02%	3.235 s
Session 2		52.3%	7.128 s
Session 1	Balloons Active Contour [40]	77.15%	3.366 s
Session 2		72.36%	5.402 s
Session 1	GVF Active Contours [41]	87.15%	4.818 s
Session 2		72.36%	6.310 s
Session 1	Proposed Active Contours without Edge	98.65%	0.003 s
Session 2		95.3%	0.010 s

(0.003s and 0.010s for Session 1 and 2 respectively).

In addition, we utilized a supervised evaluation method used by Proenca [42] to evaluate our proposed sclera segmentation method. First, we manually segmented and labelled 200 sclera images from both sessions. Then, R^2 which is an objective measure for the good-of-fit is calculated as

$$R^2 = 1 - \frac{\sum (y_i - \hat{y_i})^2}{\sum (y_i - \bar{y})^2}, \qquad (35)$$

where y_i are the desired sclera pixel values resulted from the manual segmentation, $\bar{y}$ is the mean and $\hat{y_i}$ are the actual sclera pixel values resulted from the above mentioned active contour segmentation methods. As shown in Fig. 11, our proposed method has superiority over the compared methods supporting that active contours without edge which has no stopping edge function is reliable for sclera segmentation.
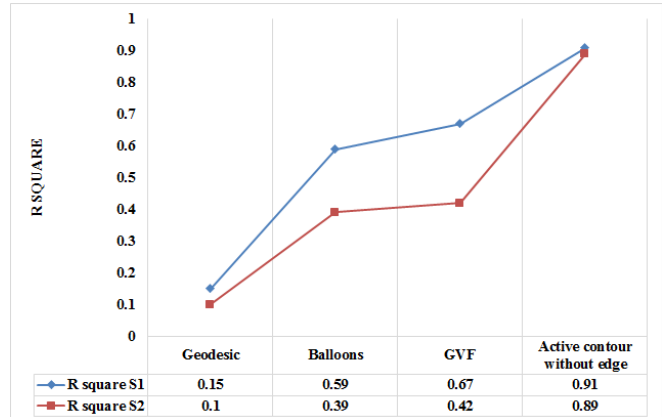

	Geodesic	Balloons	GVF	Active contour without edge
R square S1	0.15	0.59	0.67	0.91
R square S2	0.1	0.39	0.42	0.89

Fig. 11. R square values for different active contour methods evaluation at iteration $i = 200$.

3) A State-Of-The-Art Sclera Recognition Method Comparison: We compared our proposed sclera recognition method with the state-of-the-art methods on UBIRIS.v1 database as shown in Table I. In addition, we plotted the ROC curves for these comparison scenarios in Fig 13. The comparison in terms of EER includes single-Session 1 and 2, Session 1 training-Session 2 testing and Session 2 training-Session 1 testing. In terms of human supervision, the authors in [6], [11], [14], [17], [18], which their learning-based information is shown in Table I, have discarded Session 2 manually as this session has more noisy images which will affect system evaluation. While in [19], the authors stated that they used all the images even the occluded eye images but without including any occluded eye detection method. For the segmentation speed in term of active contours, [19] used a balloon-based active contour with segmentation speed of 0.14s.

In contrast, we proposed a method for occluded and partial occluded eye images which increase the robustness of the system. In addition, the segmentation speed of the proposed sclera segmentation is significantly lower (0.003s). While in terms of the non linear blood vein movement effect, the methods in [14], [17], [19] do not discuss nor suggest any method to overcome this limitation whereas our proposed system has an adaptive user template registration to extract the most homogeneous features for a final user template.
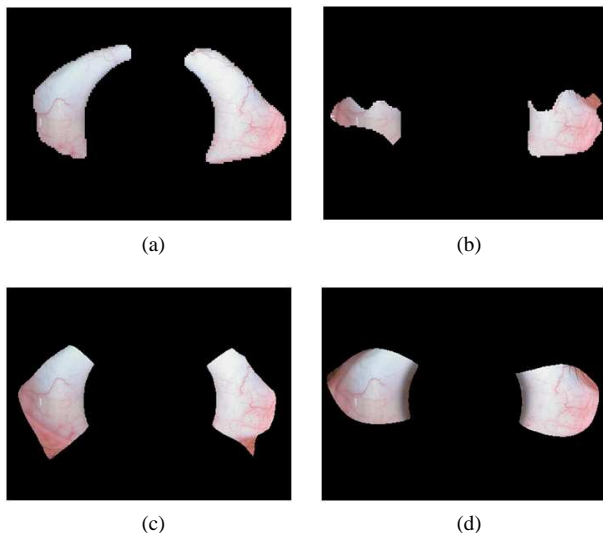
(a)   (b)

(c)   (d)

Fig. 12. The sclera regions extracted using different active contour models applied on the same image, (a) proposed active contours without edges, (b) the geodesic, (c) balloons and (d) the gradient vector flow active contours.

Fig. 13. UBIRIS.v1 ROC curve using single and multi-session comparisons.

C. Experimental Results Using the UTIRIS database

We used the UTIRIS database [44] to evaluate our proposed segmentation method accuracy. The UTIRIS database consists of two distinct sessions of visible-wavelength and near-infrared images for 79 individuals with five images from both the left and right eyes as shown in Fig. 14. We discarded the near-infrared images as our focus is on visible-wavelength images. The dimension of RGB images is 2048×1360. Some of these images are off-angle iris position which have been discarded manually. First, we resized the dimension of RGB images to 600×800 using bilinear interpolation and utilized the same evaluation process parameters as on UBIRIS.v1. As shown in Table VI, the accuracy of our proposed active contours without edges method has been decreased as compared with the UBIRIS.v1 database because some of the UTIRIS images are defocused on the sclera regions as this database is created for evaluating the iris pigmentation role in an iris recognition

TABLE IV
A STATE-OF-THE-ART COMPARISON OF RECENT WORK ON THE UBIRIS.V1 DATABASE

Method	Image discarded	EER(%) Single-session		EER(%) Multi-session	
		S1	S2	S1 training S2 testing	S2 training S1 testing
Thomas et al. [11]	Yes (S2)	3.38	n/a	n/a	n/a
Oh and Toh [14]	Yes (S2)	0.47	n/a	n/a	n/a
Zhou et al. [6]	Yes	4.09	9.98	n/a	n/a
Lin et al. [18]	Yes	3.05	n/a	n/a	n/a
Das et al. [17]	Yes (S2)	0.66	n/a	n/a	n/a
Das et al. [19]	No	0.42	0.51	3.95	4.34
Proposed method	No	2.19	2.67	3.68	4.11

4) Sclera versus Iris Recognition using the UBIRIS Database: We compared our system with the iris recognition systems using the UBIRIS.v1 database in order to analyze both iris and sclera recognition systems using visible wavelength images. For the iris recognition, two systems suggested by Proenca and Alexandre [43] and the traditional Daugman method were used. While for the sclera recognition system, the Zhou et al. [6] method was used in comparison. We used 800 images for evaluating our system since in these systems, they chose 800 images with best quality and least noise to evaluate the accuracy. In addition, we used 800 images which are randomly selected to evaluate the proposed system. As shown in Table V, our system results are better (EER=1.23%) compared to Daugman method (EER=3.72%) and to Proenca and Alexndre method (EER=2.38%) using iris in the visible wavelength. In addition, our system results are promising compared to Zhou's method in both best and random 800 images selection using proposed sclera recognition system.
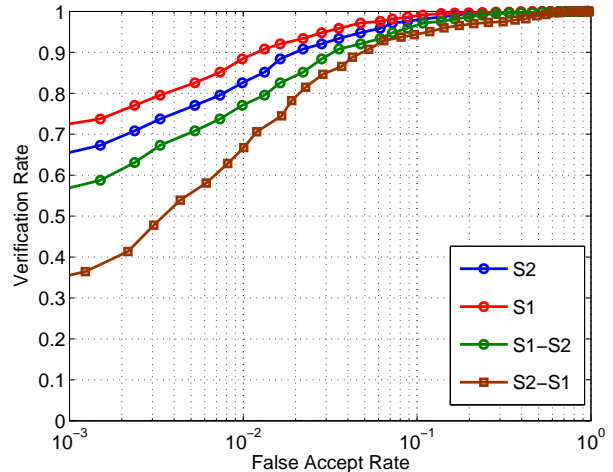
TABLE V
EER COMPARISON OF IRIS AND SCLERA RECOGNITION SYSTEMS ON UBIRIS.V1 DATABASE

Modality	Method	No. of Images	EER (%)
Iris	Proenca and Alexandre [43]	Best 800	2.38
Iris	Duagman [43]	Best 800	3.72
Sclera	Zhou *et al.* [6]	Rand 800	3.83
Sclera	Zhou *et al.* [6]	Best 800	1.34
Sclera	Our proposed system	Rand 800	2.31
Sclera	Our proposed system	Best 800	1.23

TABLE VI
COMPARISON OF SCLERA SEGMENTATION USING DIFFERENT ACTIVE
CONTOURS MODELS IN TERM OF ACCURACY AND COMPLEXITY ON UTIRIS
DATABASE

Active Contours Method	Correctly Segmented Sclera Images	Processing Time
Geodesic Active Contour [30]	66.33%	3.145 s
Balloons Active Contour [40]	71.01%	3.708 s
GVF Active Contour [41]	82.44%	4.779 s
Proposed Active Contours without Edge	90.82%	0.004 s

Fig. 15. UTIRIS database ROC curve.

system. Therefore, sclera regions are not considered important to the authors study. However, the processing time remains significantly lower compared to other active contours models. In addition, EER has been calculated (EER=6.67%) and ROC curve is shown in Fig. 15.

Fig. 14. UTIRIS right and left eye images. The upper row represents the right eye images whereas the lower row represents the left eye images.

D. Computational Load of The Proposed System

This section provides the computational load of the proposed system in each step as shown in Table VII. The properties of simulation program and PC are mentioned in the subsection VI-B2. the computational complexities of each step is calculated by running the simulation program 20 times using both UBIRIS.v1 and UTIRIS databases and the average processing time is recorded.

TABLE VII
TIME COMPLEXITY OF THE PROPOSED SYSTEM.

Sclera Recognition Steps	Complexity
Iris Segmentation	1.97 s
Sclera Validation	0.24 s
Sclera Segmentation	0.007 s
Feature Extraction	0.29 s
User Template Registration	0.46 s

E. Empirical Parameters Tuning Analysis

To analyse the tuning criteria for the system controlling parameters, we summarized these variables according to their location as follows:
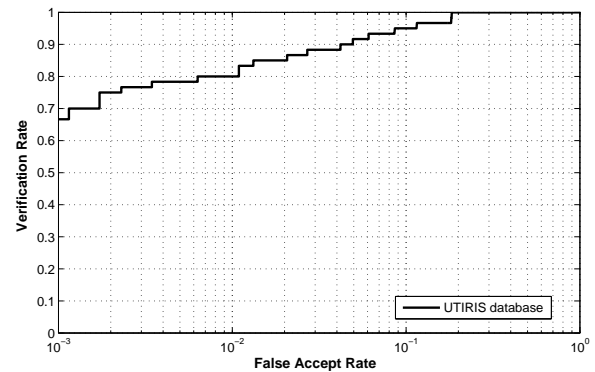
- Occluded eye detection for sclera validation: this section has three controlling parameters which are Θ, $per_{\mathbf{nsk}_{up}}$ and $per_{\mathbf{nsk}_{down}}$. For Θ, increasing the angle width provides more accurate results at the expense of processing time. While for $per_{\mathbf{nsk}_{up}}$ and $per_{\mathbf{nsk}_{down}}$, the higher the values, the more sclera samples are rejected.
- Sclera segmentation: this section has two controlling parameters which are μ and the number of iterations i. Increasing i means more curve convergence with a possibility that the fitting curve my pass through the sclera border whereas μ is discussed in subsection II-C2.
- Sclera matching and decision process: finally, the decision process is determined through first detect pair sets depending on th_p and th_ϕ whereas th_f sets the final decision. Increasing the values of th_p and th_ϕ are more likely produce false pair sets. While th_f determines FRR and FAR where the higher the th_f, the higher the FRR and the lower FAR and vice versa.

VII. CONCLUSION

In this paper, a novel occluded eye detection method has been proposed to discard the noisy images. Sclera segmentation has been achieved through an adaptive active contours without edges method. In addition, a new method for blood vein extraction and mapping have been suggested based on IUWT. For the non linear movement of the blood veins, a new user template registration is proposed to overcome this effect and create a robust sclera feature template. The results using the UBIRIS.v1 and UTIRIS databases showed that our proposed method has a lower processing time with high segmentation accuracy. In addition, the proposed method minimizes the human supervision during the recognition process introducing more robustness. This paper has not evaluated the use of off-angle sclera images which need to be considered as future work. In addition, considering different versions of the RANSAC algorithm to select the homogeneous feature sets and comparing the efficiency and processing time of each version is recommended.

funding his PhD scholarship.

REFERENCES

[1] M. Tistarelli and M. S. Nixon, *Advances in Biometrics: Third International Conferences, ICB 2009, Alghero, Italy, June 2-5, 2009, Proceedings*. Springer, 2009, vol. 5558.

[2] R. B. Hill, "Retina identification," *Biometrics: Personal Identification in Networked Society*, pp. 123–141, 2002.

[3] C.-L. Lin and K.-C. Fan, "Biometric verification using thermal images of palm-dorsa vein patterns," *IEEE Trans. Circuits Syst. Video Technol.*, vol. 14, no. 2, pp. 199–213, 2004.

[4] N. Miura, A. Nagasaka, and T. Miyatake, "Feature extraction of finger-vein patterns based on repeated line tracking and its application to personal identification," *Machine Vision and Applications*, vol. 15, no. 4, pp. 194–203, 2004.

[5] R. Derakhshani, A. Ross, and S. Crihalmeanu, "A new biometric modality based on conjunctival vasculature," *Proc. of Artificial Neural Networks in Engineering (ANNIE)*, pp. 1–8, 2006.

[6] Z. Zhou, E. Y. Du, N. L. Thomas, and E. J. Delp, "A new human identification method: sclera recognition," *IEEE Trans. Syst., Man, Cybern. A*, vol. 42, no. 3, pp. 571–583, 2012.

[7] C. Oyster, *The Human Eye: Structure And Function*. Sinauer Associates Incorporated, 1999. [Online]. Available: http://books.google.co.uk/books?id=n9yoJQAACAAJ,accessed

[8] R. Broekhuyse, "The lipid composition of aging sclera and cornea," *Ophthalmologica*, vol. 171, no. 1, pp. 82–85, 1975.

[9] R. Derakhshani and A. Ross, "A texture-based neural network classifier for biometric identification using ocular surface vasculature," in *Int. Joint Conf. on Neural Networks. IJCNN*. IEEE, 2007, pp. 2982–2987.

[10] S. Crihalmeanu and R. Derakhshani, "Enhancement and registration schemes for matching conjunctival vasculature," in *Proc. of the 3rd IAPR/IEEE International Conference on Biometrics (ICB*, 2009, pp. 1240–1249.

[11] N. L. Thomas, Y. Du, and Z. Zhou, "A new approach for sclera vein recognition," in *SPIE Defense, Security, and Sensing*. International Society for Optics and Photonics, 2010, pp. 770 805–770 805.

[12] Z. Zhou, E. Y. Du, N. L. Thomas, and E. J. Delp, "A comprehensive approach for sclera image quality measure," *International Journal of Biometrics*, vol. 5, no. 2, pp. 181–198, 2013.

[13] Z. Zhou, E. Du, C. Belcher, N. Thomas, and E. Delp, "Quality fusion based multimodal eye recognition," in *Systems, Man, and Cybernetics (SMC), 2012 IEEE International Conference on*, 2012, pp. 1297–1302.

[14] K. Oh and K.-A. Toh, "Extracting sclera features for cancelable identity verification," in *Biometrics (ICB), 2012 5th IAPR International Conference on*, 2012, pp. 245–250.

[15] M. H. Khosravi and R. Safabakhsh, "Human eye sclera detection and tracking using a modified time-adaptive self-organizing map," *Pattern Recognition*, vol. 41, no. 8, pp. 2571–2593, 2008.

[16] S. Crihalmeanu and A. Ross, "Multispectral scleral patterns for ocular biometric recognition," *Pattern Recognition Letters*, vol. 33, no. 14, pp. 1860–1869, 2012.

[17] A. Das, U. Pal, M. A. F. Ballester, and M. Blumenstein, "Sclera recognition using dense-sift," in *13th Int. Conf. on Intelligent Systems Design and Applications (ISDA)*. IEEE, 2013, pp. 74–79.

[18] Y. Lin, E. Y. Du, Z. Zhou, and N. L. Thomas, "An efficient parallel approach for sclera vein recognition," *IEEE Trans. Inf. Forensics Security*, vol. 9, no. 2, pp. 147–157, 2014.

[19] A. Das, U. Pal, M. A. F. Ballester, and M. Blumenstein, "A new efficient and adaptive sclera recognition system," in *IEEE Symp. on Computational Intelligence in Biometrics and Identity Management (CIBIM)*. IEEE, 2014, pp. 1–8.

[20] T. F. Chan and L. A. Vese, "Active contours without edges," *IEEE Trans. Image Process.*, vol. 10, no. 2, pp. 266–277, 2001.

[21] J. Daugman, "How iris recognition works," *IEEE Trans. Circuits Syst. Video Technol.*, vol. 14, no. 1, pp. 21–30, 2004.

[22] J. Daugman, "New methods in iris recognition," *IEEE Trans. Syst., Man, Cybern. B*, vol. 37, no. 5, pp. 1167–1175, 2007.

[23] W. W. Boles and B. Boashash, "A human identification technique using images of the iris and wavelet transform," *IEEE Trans. Signal Process.*, vol. 46, no. 4, pp. 1185–1188, 1998.

[24] L. Ma, T. Tan, Y. Wang, and D. Zhang, "Efficient iris recognition by characterizing key local variations," *IEEE Trans. Image Process.*, vol. 13, no. 6, pp. 739–750, 2004.

[25] R. P. Wildes, "Iris recognition: an emerging biometric technology," *Proceedings of the IEEE*, vol. 85, no. 9, pp. 1348–1363, 1997.

[26] J. Kovač, P. Peer, and F. Solina, "2d versus 3d colour space face detection," in *4th EURASIP Conf. focused on Video/Image Process. and Multimedia Commun.*, vol. 2. IEEE, 2003, pp. 449–454.

[27] M. Kass, A. Witkin, and D. Terzopoulos, "Snakes: Active contour models," *International Journal of Computer Vision*, vol. 1, no. 4, pp. 321–331, 1988.

[28] V. Caselles, F. Catté, T. Coll, and F. Dibos, "A geometric model for active contours in image processing," *Numerische Mathematik*, vol. 66, no. 1, pp. 1–31, 1993.

[29] R. Malladi, J. A. Sethian, and B. C. Vemuri, "Topology-independent shape modeling scheme," in *Int. Symp. on Optics, Imaging, and Instrumentation, SPIE*. International Society for Optics and Photonics, 1993, pp. 246–258.

[30] V. Caselles, R. Kimmel, and G. Sapiro, "Geodesic active contours," *International Journal of Computer Vision*, vol. 22, no. 1, pp. 61–79, 1997.

[31] D. Mumford and J. Shah, "Optimal approximations by piecewise smooth functions and associated variational problems," *Communications on Pure and Applied Mathematics*, vol. 42, no. 5, pp. 577–685, 1989.

[32] C. G. Owen, T. J. Ellis, A. R. Rudnicka, and E. G. Woodward, "Optimal green (red-free) digital imaging of conjunctival vasculature," *Ophthalmic and Physiological Optics*, vol. 22, no. 3, pp. 234–243, 2002.

[33] J.-L. Starck, J. Fadili, and F. Murtagh, "The undecimated wavelet decomposition and its reconstruction," *IEEE Trans. Image Process.*, vol. 16, no. 2, pp. 297–309, 2007.

[34] C. Harris and M. Stephens, "A combined corner and edge detector." in *Alvey Vision Conf.*, vol. 15, Manchester, UK, 1988, p. 50.

[35] M. Felsberg and G. Sommer, "The monogenic signal," *IEEE Trans. Signal Process.*, vol. 49, no. 12, pp. 3136–3144, 2001.

[36] M. A. Fischler and R. C. Bolles, "Random sample consensus: a paradigm for model fitting with applications to image analysis and automated cartography," *Communications of the ACM*, vol. 24, no. 6, pp. 381–395, 1981.

[37] R. Hartley and A. Zisserman, *Multiple view geometry in computer vision*. Cambridge university press, 2003.

[38] T. Dunstone, *Biometric system and data analysis: Design, evaluation, and data mining*. Springer, 2008.

[39] H. Proença and L. A. Alexandre, "Ubiris: A noisy iris image database," in *Image Analysis and Processing–ICIAP 2005*. Springer, 2005, pp. 970–977.

[40] L. D. Cohen, "On active contour models and balloons," *CVGIP: Image Understanding*, vol. 53, no. 2, pp. 211–218, 1991.

[41] N. Paragios, O. Mellina-Gottardo, and V. Ramesh, "Gradient vector flow fast geodesic active contours," in *8th IEEE Int. Conf. on Computer Vision, ICCV . Proc.*, vol. 1. IEEE, 2001, pp. 67–73.

[42] H. Proenca, "Iris recognition: On the segmentation of degraded images acquired in the visible wavelength," *Pattern Analysis and Machine Intelligence, IEEE Transactions on*, vol. 32, no. 8, pp. 1502–1516, 2010.

[43] H. Proenca and L. Alexandre, "Toward noncooperative iris recognition: A classification approach using multiple signatures," *IEEE Trans. Pattern Anal. Mach. Intell.*, vol. 29, no. 4, pp. 607–612, 2007.

[44] M. Hosseini, B. Araabi, and H. Soltanian-Zadeh, "Pigment melanin: Pattern for iris recognition," *IEEE Trans. Instrum. Meas.*, vol. 59, no. 4, pp. 792–804, 2010.

S. Alkassar received the B.Sc. degree in computer engineering from University of Technology , Baghdad, Iraq in 2006 and the M.Sc. degree in communications and signal processing from Newcastle University,Newcastle upon Tyne, U.K in 2011. He is currently working toward the Ph.D. degree in School of Electrical and Electronic Engineering, Newcastle University. His research interests include signal processing, image processing, biometrics security and pattern recognition.

W. L. Woo was born in Malaysia. He received the B.Eng. degree (1st Class Hons.) in electrical and electronics engineering and the Ph.D. degree from the Newcastle University, U.K. He was awarded the IEE Prize and the British Scholarship in 1998 to continue his research work. He is a Senior Lecturer with the School of Electrical and Electronic Engineering. Currently, he is the Director of Operations for the international branch of Newcastle University in Singapore. His major research is in the mathematical theory and algorithms for nonlinear signal and image processing. This includes areas of machine learning for signal processing, blind source separation, multidimensional signal processing, signal/image deconvolution and restoration. He has an extensive portfolio of relevant research supported by a variety of funding agencies. He has published over 250 papers on these topics on various journals and international conference proceedings. Currently, he serves on the editorial board of several international signal processing journals. He actively participate in international conferences and workshops, and serves on their organizing and technical committees. In addition, he acts as a consultant to a number of industrial companies that involve the use of statistical signal and image processing techniques. Dr Woo is a Senior Member of the IEEE and Institution Engineering Technology (IET).

S. S. Dlay Dlay received his B.Sc. (Hons.) degree in Electrical and Electronic engineering and Ph.D. degrees from Newcastle University, U.K. In recognition of his major achievements, he was appointed to a Personal Chair in Signal Processing Analysis in 2006. He has authored over 250 research papers ranging from biometrics and security, biomedical signal processing, and implementation of signal processing architectures. Professor Dlay serves on many editorial boards and has played an active role in numerous international conferences in terms of serving on technical and advisory committees as well as organizing special sessions.

J. A. Chambers (S'83-M'90-SM'98-F'11) received the Ph.D. and D.Sc. degrees in signal processing from the Imperial College of Science, Technology and Medicine (Imperial College London), London, U.K., in 1990 and 2014, respectively. He is a Professor of signal and information processing within the School of Electrical and Electronic Engineering, Newcastle University, U.K., and a Fellow of the Royal Academy of Engineering, U.K.. He has also served as an Associate Editor for the IEEE TRANSACTIONS ON SIGNAL PROCESSING over the periods 1997-1999, 2004-2007, and as a Senior Area Editor 2011-15.